0026-895X/05/6704-1078–1088
MOLECULAR PHARMACOLOGY
U.S. Government work not protected by U.S. copyright
Mol Pharmacol 67:1078–1088, 2005

Vol. 67, No. 4
10108/1197657
Printed in U.S.A.

Molecular Determinants of the Agonist Binding Domain of a P2X Receptor Channel

Zonghe Yan, Zhaodong Liang, Melanija Tomić, Tomas Obsil, and Stanko S. Stojilkovic

Section on Cellular Signaling, Endocrinology and Reproduction Research Branch, National Institute of Child Health and Human Development, National Institutes of Health, Bethesda, Maryland (Z.Y., Z.L., M.T., S.S.S.); and Department of Physical and Macromolecular Chemistry, Faculty of Science, Charles University, Prague, Czech Republic (T.O.)

Received December 7, 2004; accepted January 4, 2005

ABSTRACT

P2 purinergic receptor channel receptors (P2XRs) are a family of ligand-gated cation channels composed of two transmembrane domains, N and C termini located intracellularly, and a large extracellular loop containing the ATP binding domain. To identify regions important for binding and gating, previous experimental work was focused on mutagenesis of conserved ectodomain residues. Here, we used the known sequence and secondary structure similarities between the Lys180-Lys326 ectodomain region of $P2X_4$ and the class II aminoacyl-tRNA synthetases as a guide to generate a three-dimensional model of the receptor-binding site and to design mutants. The interplay between homology modeling and site-directed mutagenesis suggested that Asp280 residue of $P2X_4R$ coordinates ATP binding via the magnesium ion, Phe230 residue coordinates the binding of the adenine ring of ATP, and Lys190, His286, and Arg278 residues coordinate the actions of negatively charged α-, β-, and γ-phosphate groups, respectively. Until the crystal structure of the channel is solved, this model could provide a useful approach for future studies on the identification of ATP binding domain and gating of P2XRs.

P2X receptors (P2XRs) are a family of ATP-gated cation channels composed of seven receptor subunits, termed $P2X_{1-7}$ (Ralevic and Burnstock, 1998; North, 2002). Each subunit is composed of two transmembrane domains, placing N and C termini intracellularly and most of the protein extracellularly (Newbolt et al., 1998). The trimeric homo- or heteromeric assembly of subunits organized in a head-to-tail orientation around the central pore most likely accounts for the formation of functional P2XRs (Nicke et al., 1998; Jiang et al., 2003). Among subunits, the C termini vary in their structure and length (North, 2002) and contain several motifs involved in receptor desensitization (Koshimizu et al., 1999). The ectodomain is glycosylated (Rettinger et al., 2000; Hu et al., 2002) and includes 10 conserved cysteine residues, probably forming disulfide bonds and contributing to the tertiary structure of the receptor (Ennion et al., 2001; Clyne et al., 2002b). Approximately 80 other extracellular residues are also conserved in at least six subunits. The ectodomain contains the ligand binding pocket and structural elements that influence receptor deactivation and desensitization rates (Fabbretti et al., 2004; Sokolova et al., 2004; Zemkova et al., 2004). The three-dimensional structure of P2XRs is unknown, and it has not been determined whether ligand binding domain is within inter- or intrasubunits. However, it is well established that the constituent components of ATP show no agonist or antagonist actions at P2XRs, indicating that both the adenine ring and the triphosphate chain are critical for high-affinity binding (North, 2002). It is also established that P2XRs are regulated allosterically by protons, divalent cations, and metals (Li et al., 1997; Wildman et al., 1999; Clarke et al., 2000; Negulyaev and Markwardt, 2000; Clyne et al., 2002a; Coddou et al., 2003).

At present, there are three models that describe ATP binding site at P2XRs. Evans and collaborators developed a model of ATP binding pocket derived from data from site-directed mutagenesis of human $P2X_1R$ (Vial et al., 2004). Mutation of aromatic amino acids at this receptor indicated the relevance of two residues, Phe185 and Phe291, in ATP action (Roberts and Evans, 2004). This finding is consistent with a hypothesis that adenine moiety of an ATP molecule is sandwiched between these two residues, similar to that observed in crystal structure of 5′-nucleotidase (Knofel and Strater, 2001). Furthermore, three conserved positively charged residues, Lys68, Arg292, and Lys309, that are close to the vestibule of the ionic pore, seem to be associated with the binding of the phosphate chain of ATP (Ennion et al., 2000). This model does not include a role for Mg^{2+} in coordination of ATP

Article, publication date, and citation information can be found at http://molpharm.aspetjournals.org.
doi:10.1124/mol.104.010108.

ABBREVIATIONS: P2XR, P2 purinergic receptor channel; GFP, green fluorescent protein; τ_{des}, rate of receptor desensitization; 2-MeS-ATP, 2-methylthio ATP tetrasodium; Bz, benzoylbenzolyl; HEK, human embryonic kidney.

binding (Vial et al., 2004), because experimental data revealed no effects of mutation of numerous negatively charged residues on ATP potency (Ennion et al., 2001).

Freist and collaborators (1998) and Mager et al. (2004) developed theoretical models of the ATP binding site. Freist's model is derived from sequence alignments and secondary structure predictions between class II aminoacyl-tRNA synthetases and P2XRs. This model has not been experimentally tested, presumably because the sequence alignment between the enzyme and P2XRs is relatively poor. However, several residues predicted by sequence alignment to participate in ATP binding have been mutated in studies on conserved residues in ectodomains of human $P2X_1$ and rat $P2X_2$ subunits. Consistent with the model, mutation of Lys188 at $P2X_2R$, the corresponding residue for recognition of γ-phosphate, produced a rightward shift in the sensitivity of receptors to ATP (Jiang et al., 2000). Furthermore, the responsiveness to ATP was abolished by mutation of Phe227, the potential residue for adenosine recognition (Nakazawa et al., 2004). At $P2X_1R$, mutation of Lys190 also produced a rightward shift in the sensitivity, whereas ATP potency was not affected by substitution of Arg314, the potential residue for recognition of γ-phosphate (Ennion et al., 2000), and Phe230, the potential residue for adenosine recognition (Roberts and Evans, 2004).

Here, we tested Freist's model by mutating Lys190, Lys197, Phe230, Asp280, and Arg318 residues of rat $P2X_4R$. Using the crystal structures of several class II aminoacyl-tRNA synthetases as templates, we also built a three-dimensional model of the Lys180-Lys326 ectodomain region of $P2X_4$ and identified and mutated four additional residues that could participate in ATP binding. The interplay between homology modeling and mutagenesis indicates which residues participate in ATP binding at $P2X_4R$ and provides a useful framework for the identification of ligand binding pocket at other subunits.

Materials and Methods

DNA Constructs, Site-Directed Mutagenesis, Cell Culture, and Transfection. The C-terminal GFP-tagged $P2X_4$ construct was generated through deleting sequences between the C terminus of coding sequences of subcloned $P2X_4$ cDNA and the initiation codon of GFP gene in the previously described $P2X_4$-biscistronic enhanced green fluorescent protein expression vector (pIRES2-EGFP) construct (He et al., 2003b), mainly including the internal ribosome entry site. Deletion was created using the QuikChange XL site-directed mutagenesis kit (Stratagene, La Jolla, CA) according to the manufacturer's instructions and 5′-ctttcgggggagatgaaccagatggtgagcaagggcgaggag-3′ and 5′-ctcctcgcccttgctcaccatctggttcatctcccccgaaag-3′ as the mutagenic oligonucleotide primers, synthesized and polyacrylamide gel electrophoresis-purified by Integrated DNA Technology (Coralville, IA). Both the C-terminal GFP-tagged $P2X_4$ and $P2X_4$/pIRES2-EGFP construct were used as templates for production of plasmids containing the specific amino acid residue point mutation of $P2X_4$ cDNA. The point mutations were introduced using the QuikChange XL site-directed mutagenesis kit. Productions of the correct C-terminal GFP-tagged $P2X_4$ constructs, mutations, and absence of coding errors in these constructs were verified by dye terminator-cycle sequencing (PerkinElmer Life and Analytical Sciences, Boston MA; performed by Veritas, Inc., Rockville, MD). Large-scale plasmid DNAs were prepared using a QIAfilter Plasmid Maxi kit (QIAGEN, Valencia, CA). Mouse immortalized gonadotropin-releasing hormone-secreting GT1–7 cells and human embryonic kidney (HEK) 293 cells were used for the expression of wild-type and mutant $P2X_4$ receptors, as described previously (He et al., 2003a). GT1–7 and HEK293 cells were routinely maintained in Dulbecco's modified Eagle's medium/Ham's F-12 medium (1:1) containing 10% (v/v) fetal bovine serum (Biofluids, Rockville, MD) and 100 μg/ml gentamicin (Invitrogen, Carlsbad, CA) in a water-saturated atmosphere of 5% CO_2 and 95% air at 37°C. Cells were plated on 25-mm poly-L-lysine (0.01% w/v; Sigma-Aldrich, St. Louis, MO)-coated coverslips at a density of 0.1×10^6 cells for current recording and 0.5×10^6 cells for calcium measurement per 35-mm dish. The transient transfection was conducted 24 h after plating the cells using 2 μg of DNA and 5 μl of LipofectAMINE 2000 reagent (Invitrogen) in 2 ml of serum-free Opti-MEM. After 4.5 h of incubation, the transfection mixture was replaced with normal culture medium. Cells were subjected to experiments 24 to 48 h after transfection.

Calcium Measurements. Transfected GT1–7 cells were preloaded with 1 μM Fura-2/acetoxymethyl ester (Molecular Probes, Eugene, OR) for 60 min at room temperature in modified Krebs-Ringer buffer: 120 mM NaCl, 5 mM KCl, 1.2 mM $CaCl_2$, 0.7 mM $MgSO_4$, 15 mM HEPES, and 1.8 g/liter glucose, pH 7.4. After dye-loading, cells were incubated in modified Krebs-Ringer buffer and kept in the dark for at least 30 min before $[Ca^{2+}]_i$ measurements. Coverslips with cells were mounted on the stage of an Eclipse TE 200 microscope (Nikon, Japan) attached to the PTI IC-300 fluorescence system (Photon Technology International, Monmouth Junction, NJ). Cells were stimulated with various doses of agonists, the dynamic changes of $[Ca^{2+}]_i$ were examined under an ×40 oil immersion objective during exposure to alternating 340- and 380-nm excitation light beams, and the intensity of light emission at 520 nm was measured. The F_{340}/F_{380} ratio of light intensities, which reflects changes in $[Ca^{2+}]_i$, was simultaneously followed in 15 to 50 cells. Cells expressing GFP were optically detected by an emission signal at 520 nm when excited by a 488-nm light. Experiments were done in cells with comparable GFP fluorescence signals (approximately 5 arbitrary units at 0–10 scale), and no repetitive stimulation was done to avoid the possible impact of desensitization on the amplitude and pattern of $[Ca^{2+}]_i$ signals.

Current Measurements. Electrophysiological experiments were performed on HEK293 cells at room temperature using whole-cell patch-clamp recording techniques. ATP-induced currents were recorded using an Axopatch 200B patch clamp amplifier (Axon Instruments Inc., Union City, CA) and were filtered at 2 kHz using a low-pass Bessel filter. Patch electrodes, fabricated from borosilicate glass (type 1B150F-3; World Precision Instruments, Inc., Sarasota, FL) using a Flaming Brown horizontal puller (P-87; Sutter Instruments, Novato, CA), were heat-polished to a final tip resistance of 4 to 6 MΩ. All current records were captured and stored using the pClamp 8 software packages in conjunction with the Digidata 1322A A/D converter (Axon Instruments). In general accordance with literature (Jiang et al., 2003), patch electrodes were filled with a solution containing 142 mM NaCl, 1 mM $MgCl_2$, 10 mM EGTA, and 10 mM HEPES; the pH was adjusted with 10 M NaOH to 7.35. The osmolarity of the internal solutions was 306 mOsM. The bath solution contained 142 mM NaCl, 3 mM KCl, 1 mM $MgCl_2$, 2 mM $CaCl_2$, 10 mM glucose, and 10 mM HEPES; the pH was adjusted to 7.35 with 10 M NaOH. The osmolarity of this solution was 295 to 305 mOsM. ATP was daily prepared in bath buffer with pH properly readjusted and applied using a fast gravity-driven microperfusion system (BPS-8; ALA Scientific Instruments, Westbury, NY). The current responses were recorded from single spherical cells clamped at –60 mV. The impact of expression level on current was reduced by selecting cells with comparable $P2X_4$ fused GFP fluorescence before immersing the electrode in bath solution for gigaohm seal. Responses were normalized to cell membrane capacitance (in a range of 7–23 pF) and presented as current density (in picoamperes per picofarads). Dose-response data were collected from recordings of a range of ATP concentration buffers applied to single cells with a washout interval of 5 min between each application, and the corresponding currents were normalized to the highest current amplitude. The pH sensitivity of receptors was tested by repetitive application of ATP at

pH 6.50, 7.35, and 8.00, with pH buffer equilibration for 1 min before agonist application.

Confocal Microscopy. The distribution of GFP-tagged receptors within live cells was examined by laser scanning confocal microscopy. HEK293 cells were cultured on poly-L-lysine–coated coverslips (0.1×10^6 cells/dish), transfected, and imaged the next day. The culturing medium was replaced with phenol red and ATP-free Krebs-Ringer buffer, and coverslips with cells were mounted on the stage of an inverted microscope (Nikon Diaphot 300) attached to an MRC 1024 system (Bio-Rad, Hercules, CA). Images were collected under 60× objective lens, and further zoom (3×) was also applied.

Modeling of P2X Ectodomain. Three-dimensional model of rat $P2X_4$ Lys180–Lys326 ectodomain region was generated using the SWISS-MODEL server (Schwede et al., 2003) and crystal structures of seryl-tRNA synthetase (PDB code 1SES), glycyl-tRNA synthetase (PDB code 1B76), and histidyl-tRNA synthetase (PDB code 1KMN) as templates (Belrhali et al., 1994; Arnez et al., 1997, 1999). The secondary structure of rat $P2X_4$ sequence was predicted using the PSI-PRED algorithm (Jones, 1999). Sequence and secondary structure homology between P2XRs and the class II aminoacyl-tRNA synthetases (Freist et al., 1998) was used to build a three-dimensional model of rat $P2X_4$-Lys180–Lys326 ectodomain region using the DeepView/Swiss-PdbViewer v3.7 program (Guex and Peitsch, 1997). The final model was validated by PROCHECK, and bad contacts were corrected manually by O program (Jones et al., 1991). Disulphide bridges Cys217–Cys227 and Cys261–Cys270 were created using O program. The resulting model was then energy-minimized using GROMACS package (http://www.gromacs.org) with the parameters set at ffG43a1. The ligand docking started with manual docking of ATP molecule into the predicted binding site of rat $P2X_4$ Lys180–Lys326 ectodomain model on the basis of homology with class II aminoacyl-tRNA synthetases. Subsequently, the geometric recognition algorithm implemented in the docking program GRAMM (Katchalski-Katzir et al., 1992) and GHEMICAL modeling package (Hassinen and Perakyla, 2001) were used to refine the structure of $P2X_4$-ATP complex.

Calculations. Whenever appropriate, the data were presented as mean ± S.E.M. The time course of the current and $[Ca^{2+}]_i$ was fitted by one-phase exponential decay function ($ae^{-kt} + b$; where $k = 1/\tau_{des}$) using the pClamp 8 program (Axon Instruments) and Prism 4 (GraphPad Software Inc., San Diego, CA), respectively. Significant differences, with $P < 0.01$, were determined by Mann-Whitney test using GraphPad InStat 3.05. Concentration-response data were fitted by a four-parameter logistic equation using a nonlinear curve-fitting program that derives EC_{50} values (Kaleidagraph; Sinergy Software, Reading, PA).

Results

Experimental Considerations. To visualize the expression pattern of wild-type and mutant $P2X_4$Rs, the sequence for enhanced GFP was tagged to the C terminus of $P2X_4$R as described under *Materials and Methods,* and both fused and nonfused receptors were expressed in HEK293 and GT1–7 cells. As shown in Fig. 1A, left, GFP translated from the same bicistronic mRNA as $P2X_4$R was homogeneously distributed within the HEK293 cells. The $P2X_4$R-fused GFP was also expressed, but it was localized in the plasma membrane and in intracellular structures, presumably Golgi apparatus and

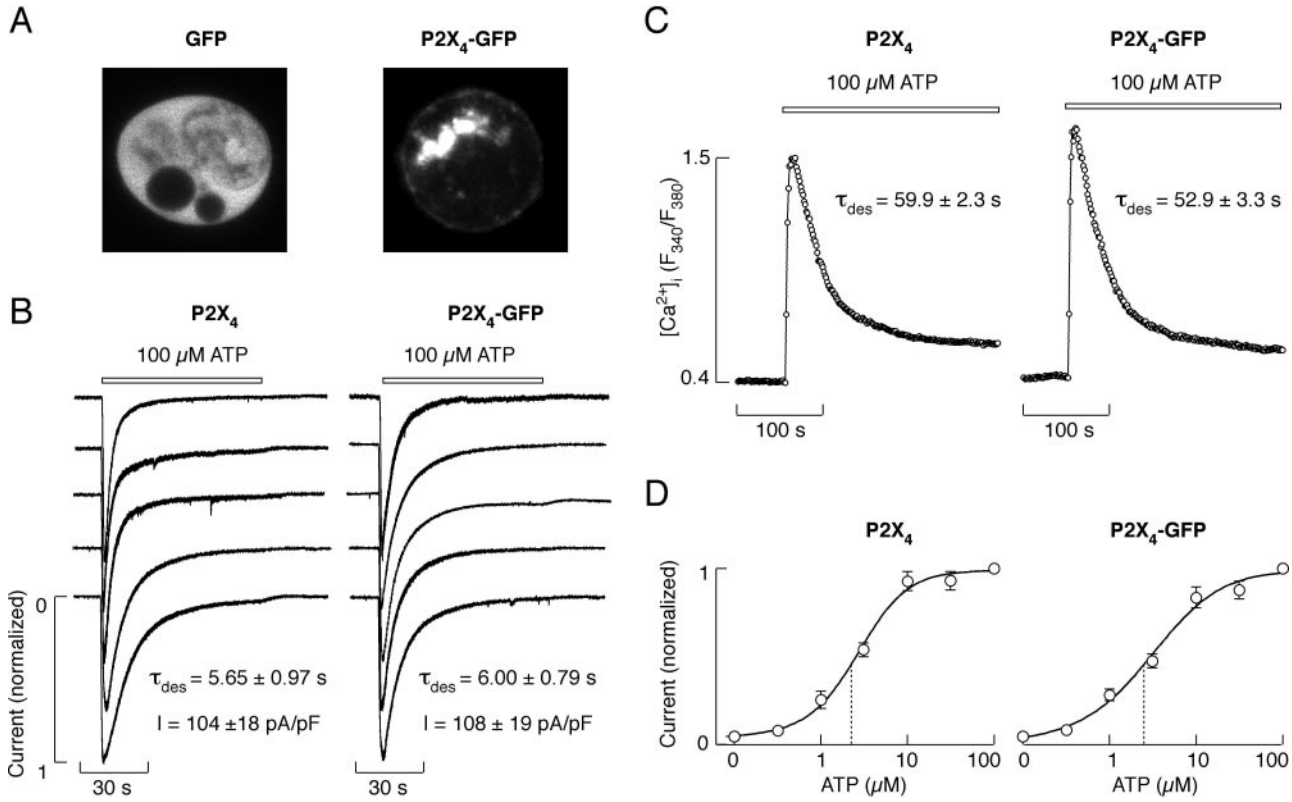

Fig. 1. Attachment of GFP to C-terminal does not affect the expression and gating of $P2X_4$R. A, confocal images of GFP fluorescence in transfected HEK293 cells. Distribution of GFP without $P2X_4$ fusion (left) and $P2X_4$-fused GFP (right). B, typical patterns of ATP-induced currents in HEK293 cells expressing $P2X_4$ (left) and GFP-tagged $P2X_4$ (right) receptors. Traces shown are from different cells. The numbers below the traces show mean values ± S.E.M. for time constants of receptor desensitization (τ_{des}) and peak amplitude (I). C, ATP-induced calcium responses in GT1–7 neurons expressing $P2X_4$ (left) and $P2X_4$-GFP (right) receptors. Traces shown are means from 20 cells in a representative sample from 10 experiments. Numbers above the traces indicate time constants of calcium-signal desensitization. D, concentration-dependent effects of ATP on peak current responses in HEK293 cells expressing $P2X_4$ (left) and $P2X_4$-GFP (right). Broken lines denote EC_{50} values.

vesicles (Fig. 1A, right), presumably endosomes (Bobanovic et al., 2000). Consistent with the plasma-membrane expression of $P2X_4$-GFP in HEK293 cells, ATP in 0.5 to 100 μM concentration range always triggered an inward current in GFP-positive cells. Figure 1B shows typical current traces elicited by 100 μM ATP in five cells expressing $P2X_4R$ (left) and five cells expressing the GFP-tagged $P2X_4R$ (right). These and all other experiments were done in cells with comparable GFP fluorescence signals (approximately 5 arbitrary units at 0–10 scale). There was no obvious difference in the rise time and peak amplitude of current responses (Fig. 1B, I) between two receptors. In addition, in all cases monoexponential decays of current were observed with highly comparable time constants of desensitization (Fig. 1B, τ_{des}).

In further experiments, we analyzed the patterns of calcium signaling by two receptors. HEK293 cells endogenously express calcium-mobilizing P2Y receptors, and their coactivation interferes with calcium influx-dependent signaling (He et al., 2003a). To avoid this, we used GT1–7 neurons, which do not express P2XRs or P2 purinergic G protein-coupled receptors endogenously (Koshimizu et al., 1998). The patterns of calcium signaling by two receptors were highly comparable independently of the status of voltage-gated Ca^{2+} influx. Figure 1C illustrates a typical pattern of the increase in intracellular calcium concentration ($[Ca^{2+}]_i$) in cells without blockade of voltage-gated Ca^{2+} influx. The rise times and average peak amplitudes of calcium signals were similar, as were the time constants of calcium signal desensitization during continuous application of ATP. Finally, concentration-dependent studies using current (Fig. 1D) and calcium (data not shown) measurements revealed that the potency of ATP for two receptors was similar. All together, these results indicate that the attachment of GFP does not obviously affect receptor expression and pharmacological and kinetic properties, but it provides a useful method to clarify the plasma-membrane expression of protein.

Characterization of Mutants Predicted by Freist's Alignment Model. In Freist's model, the highly conserved Lys190 residue of $P2X_4R$ accounts for binding of the α-phosphate moiety of ATP, whereas Lys197 and Arg318 participate in binding of the γ-phosphate moiety of ATP. The relevance of these residues was tested by generating the following mutants of the $P2X_4$ subunit: K190A, K190R, K197A, R318A, and R318K. The K197A mutant was functional, and ATP potency and the rate of receptor desensitization were not obviously affected (Table 1). In contrast, 3 of 11 cells expressing the K190A mutant did not respond to the application of 100 μM ATP (Fig. 2B), whereas the residual cells responded with peak current representing approximately 1% of that observed in controls (Table 1). A decrease in responsiveness of this mutant did not result from trafficking problems, because the receptor exhibited a typical pattern of plasma-membrane expression (Fig. 2A). In addition, a fraction of mutated receptors not fused with GFP did not respond to 100 μM ATP application, whereas the residual cells responded with low amplitude signals (data not shown). All cells expressing the K190A mutant responded to 5 mM ATP with higher current amplitude (Fig. 2C) but not to application of 100 μM 2-MeS-ATP and BzATP (data not shown), indicating a rightward shift in the sensitivity of receptors to agonists. The receptor function was preserved in the K190R mutant (Fig. 2B), confirming the importance of a positively charged residue at this position. As shown in Fig. 2D, the K190R receptor responded to ATP application in a dose-dependent manner, with an EC_{50} value shifted slightly rightward from the control EC_{50} (Table 1). The peak amplitude of K190R current induced by 100 μM ATP was approximately 50% of the wild-type channel, whereas the rates of receptor desensitization were not influenced (Table 1).

The plasma membrane expression pattern of R318A mutant was normal (Fig. 3A). However, the receptor showed a significant reduction in the peak current when stimulated

TABLE 1

Characterization of ATP-induced currents in HEK293 cells expressing wild-type and mutant rat $P2X_4$ receptors

Peak current values and τ_{des} values were derived from responses to 100 μM ATP. Data shown are means ± S.E.M.. The number of experiments per group varied between 5 and 15.

$P2X_4$ Channels	EC_{50}	Peak Current Amplitude	τ_{des}
	μM	pA/pF	s
Wild-type	3.0 ± 0.5	82.9 ± 9.4	5.7 ± 0.6
K190A	>5000	0.9 ± 0.4	
K190R	6.7 ± 0.6*	44.7 ± 7.2*	5.9 ± 1.1
K197A	3.8 ± 0.8	32.4 ± 3.1*	4.8 ± 0.8
F230A	>5000	1.5 ± 0.4*	
F230W	3.9 ± 0.6	67.1 ± 8.3	6.1 ± 1.2
F230Y	5.9 ± 1.3	67.7 ± 11.7	6.7 ± 2.2
K258A	3.8 ± 1.4	70.4 ± 9.9	4.7 ± 0.8
R278A	>5000	3.7 ± 0.6*	
R278K	1.9 ± 0.3	43.4 ± 1.7*	4.5 ± 0.6
D280A	>5000	3.7 ± 0.9*	
D280Q	>5000	1.4 ± 0.5*	
D280E	3.6 ± 0.4	41.1 ± 9.8*	6.4 ± 0.7
H286A	3.7 ± 0.7	38.8 ± 6.2*	3.7 ± 0.7
N287A	5.8 ± 0.8	34.9 ± 4.9*	7.3 ± 1.4
R318A	59 ± 9.5*	36.5 ± 8.8*	6.6 ± 1.4
R318K	1.2 ± 0.3	56.3 ± 19.4	5.8 ± 0.6

* $P < 0.01$ versus wild-type channel.

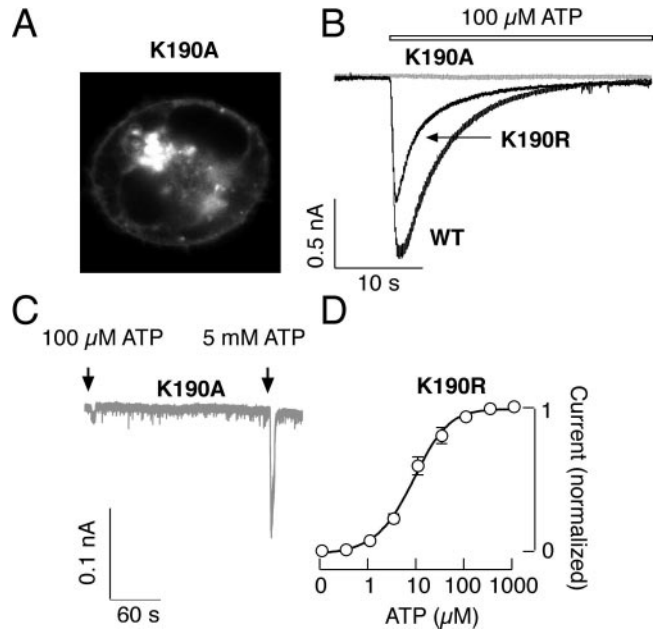

Fig. 2. Characterization of Lys190 mutant $P2X_4$ receptors. A, the expression pattern of mutant receptors. B, typical patterns of current signals of wild-type and mutant receptors in response to 100 μM. C, current responses to two ATP concentrations. D, dose-dependent effects of ATP on peak current response by rescue K190R mutant. Data points are mean values ± S.E.M.

with 100 μM ATP (Fig. 3, B and C, and Table 1). Dose-dependent studies revealed a 20-fold decrease in the potency of ATP for the mutant receptor compared with the wild-type receptor (Fig. 3D). The relevance of a positively charged residue at this position was further indicated by replacement of arginine with lysine. The potency of ATP for R318K mutant was slightly shifted leftward (Fig. 3D), whereas the peak current amplitude was not significantly different from that observed in wild-type channels (Fig. 3, B and C, and Table 1). Change in ATP potency reflects the amount of ATP required to induce the channel opening but does not clarify which step in the activation of receptors, a decrease in the binding affinity of receptor and/or the functional translation of agonist binding to the gating, accounts for this shift. However, partial agonist may be able to discriminate between mutations that affect agonist binding versus P2XR-channel gating (Roberts and Evans, 2004). For $P2X_4R$, $\alpha\beta$-MeATP acts as a partial agonist (Khakh et al., 1999). As shown in Fig. 3E, the peak amplitude of current response of wild-type $P2X_4R$ to 1 mM $\alpha\beta$-MeATP was approximately 40% of that observed in response to stimulation with 100 μM ATP. Furthermore, the wild-type and mutant channels showed similar EC_{50} values when stimulated with $\alpha\beta$-MeATP (Fig. 3F). These observations are more consistent with the role of the Arg318 residue in signal transduction than agonist binding.

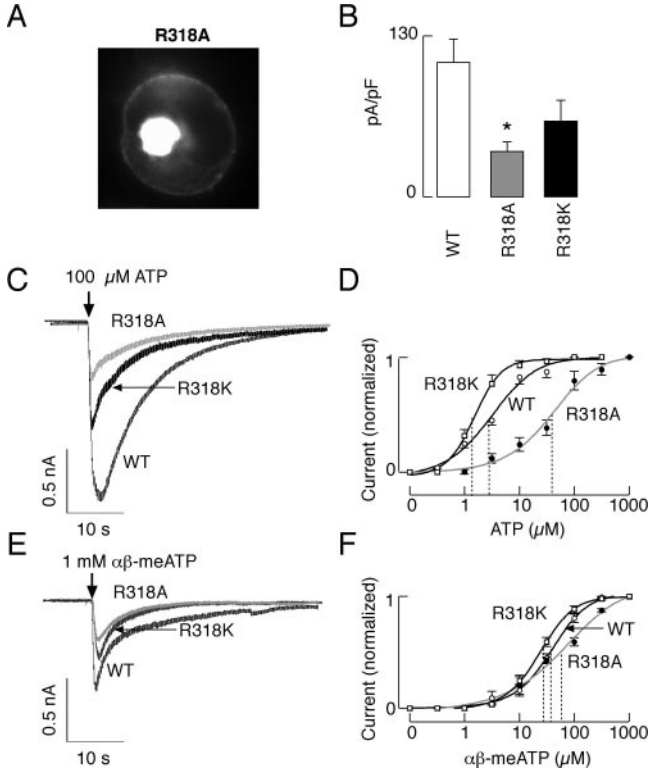

Fig. 3. Arg318 may participate in signal transduction. A, expression pattern of R318A mutant in HEK293 cells. B, mean values of peak current amplitudes in response to 100 μM ATP. ⋆, significant differences between wild-type and R318A (▤) and R318K (■) mutant receptors. C, typical patterns of ATP (100 μM)-induced current signals in HEK293 cells expressing wild-type and R318A (gray trace) and R318K (black trace) mutants. D, concentration-dependent effects of ATP on peak current amplitude of wild-type and mutant receptors. E, representative traces of currents by wild-type and mutant receptors in response to stimulation with 1 mM $\alpha\beta$-MeATP. F, concentration-response curves for wild-type and Arg318 mutants in response to stimulation with $\alpha\beta$-MeATP. Vertical broken lines illustrate EC_{50} values.

The predicted residue by Freist's model for Mg^{2+} binding at $P2X_4R$ is Asp280. To neutralize the negative charge of this residue, we generated two mutants, D280A and D280Q. Both mutants were expressed at the plasma membrane in a manner highly comparable with that observed with wild-type receptors (Fig. 4, A and B, left). Mutants also responded to the application ATP but with a small current (Fig. 4, A and B, center and right). The peak current amplitude induced by 100 μM ATP represented approximately 4% of that seen with wild-type receptors. Increase in ATP concentrations up to 5 mM only slightly (2- to 3-fold) increased the amplitude of current (Fig. 4, A and B, right). In concentrations greater than 5 mM, ATP permeabilized cells independently of the expression of P2XRs. When added in 100 μM concentrations, BzATP and 2-MeS-ATP induced currents of amplitudes and profiles comparable with 100 μM ATP. Similar results were observed with mutant receptors not tagged to GFP, as well as in GFP-tagged and nontagged mutant receptors when expressed in GT1–7 cells (data not shown).

To further test the relevance of a negatively charged residue at this position for ATP action, we generated the "rescue" D280E-$P2X_4$ mutant. As shown in Fig. 4C, left, this mutant expressed in HEK293 cells responded to ATP stimulation with a current similar to that observed in cells expressing wild-type channels. The mutant receptor also responded to 100 μM ATP with an increase in $[Ca^{2+}]_i$ when expressed in GT1–7 cells (Fig. 4C, center). At an ATP concentration of 100 μM, the peak of current signals was lower compared with that of the wild-type receptor, but the rate of receptor desensitization was not affected (Table 1). The dose-response studies revealed a typical pattern of response (Fig. 4C, right), with an estimated EC_{50} value comparable with that observed in cells expressing wild-type receptors (Table 1).

According to Freist's alignment model, Phe230 should play a role at $P2X_4R$ in recognition of the adenine group of ATP. Consistent with this prediction, the F230A mutant of $P2X_4R$ showed a small (less than 2–3% of that observed in controls) peak current response in 15 of 17 GFP-positive cells stimulated with 100 μM ATP (Fig. 5, B and C, and Table 1). A similar pattern of response was observed during the application of 100 μM 2-MeS-ATP and BzATP. The low responsiveness of this mutant did not result from its miss-expression, because it is indicated by localization of GFP fluorescence at the plasma membrane (Fig. 5A). Elevation in ATP concentrations to up to 5 mM was associated with an increase in the peak current amplitude (Fig. 5C), further indicating the functional assemble of mutant subunits at the plasma membrane. Because of the nonspecific effects of millimolar ATP concentrations, we were unable to estimate the EC_{50} values for this mutant. The replacement of phenylalanine with tryptophan and tyrosine "rescued" the function of channels, indicating the importance of an aromatic residue in that position (Fig. 5, D and E). The amplitude of current response by F230W and F230Y mutants was approximately 80% of that observed in wild-type channels, whereas the rates of current desensitization for these two mutants were not affected (Table 1). Both mutants responded to ATP in a typical dose-dependent manner (Fig. 5F), with EC_{50} values comparable with those observed in cells expressing wild-type channels (Table 1).

Three-Dimensional Model of $P2X_4R$. We used several X-ray structures of aminoacyl-tRNA synthetases as templates for three-dimensional homology modeling of the 180 to

326 $P2X_4$ ectodomain fragment. As shown in Fig. 6A, the class II enzymes possesses a unique fold with a catalytic domain built on six-stranded antiparallel β-sheets surrounded by α-helices and contains three homologous sequences, termed motifs 1, 2, and 3 (Eriani et al., 1995). Three amino acid residues at motif 2 and one residue at motif 3 form an ATP binding site (Arnez et al., 1997). Our model of the $P2X_4R$ 180 to 326 fragment also adopts a six-stranded β-pleated sheet structure and contains an ATP binding site (Fig. 6B). However, the molecule of ATP docked within the ligand-binding site of $P2X_4$ ectodomain model adopts more extended conformation compared with the class II aminoacyl-tRNA synthetases. In addition, notice the difference in lengths of a large loop between β1 and β2 strands and the α-helix between β2 and β3 strands in the sequences of the enzyme and $P2X_4R$ (Fig. 6B).

The details of the enzyme's ATP binding pocket are shown in Fig. 6, C and E. The adenine base of ATP stacks over the invariant phenylalanine residue from motif 2 and the α-phosphate interacts with the first conserved arginine of motif 2, whereas the second highly conserved arginine of motif 2 and the completely conserved arginine of motif 3 interact with the γ-phosphate. The predicted ligand-binding pocket of $P2X_4R$ incorporates three of five residues indicated by Freist's alignment model: Asp280, Phe230, and Lys190. ATP is cradled by the antiparallel β-sheets, and the adenine base stacks over the Phe230 residue (Fig. 6, D and F). The aspartate 280 of the β4 strand binds to the magnesium ion, which is modeled between this residue and the γ-phosphate group of ATP. This interaction mimics the binding of Asp293 to the magnesium ion of an ATP-Mg^{2+} complex in the enzyme structure. The Lys190 residue of $P2X_4$ subunit located within the β1 strand interacts with the α-phosphate.

Contrary to Freist's alignment model, in our three-dimensional model, the β4-strand residue Arg278 interacts with the γ-phosphate, and the His286 residue located on the beginning of β5 strand, and/or nearby Lys258 or Asn287 residues, interacts with the β-phosphate group of ATP. The difference in the length of a large loop between β1 and β2 strands in the sequences of the enzyme and channel underlies a shift of residues contributing to the recognition of the phosphate chain of ATP (Fig. 6B). This provides a rationale for the lack of effects of a K197A mutation on the channel function (Table 1). Arg318 is the last $P2X_4$ residue predicted by Freist's model to be near ATP. However, our model indicates that if Arg318 residue participates in ligand binding, it could be in contact with the deoxyribose ring rather than with the γ-phosphate of ATP (Fig. 6, D and F). The incorporation of this residue in α-helix is also consistent with our observation of the potential role of this segment in transduction of signaling toward the second transmembrane domain (Fig. 3). Finally, our model includes two disulphide bridges: the Cys217–Cys227 and Cys261–Cys270 (shown in orange in Fig. 6D). No large structural changes were necessary to cre-

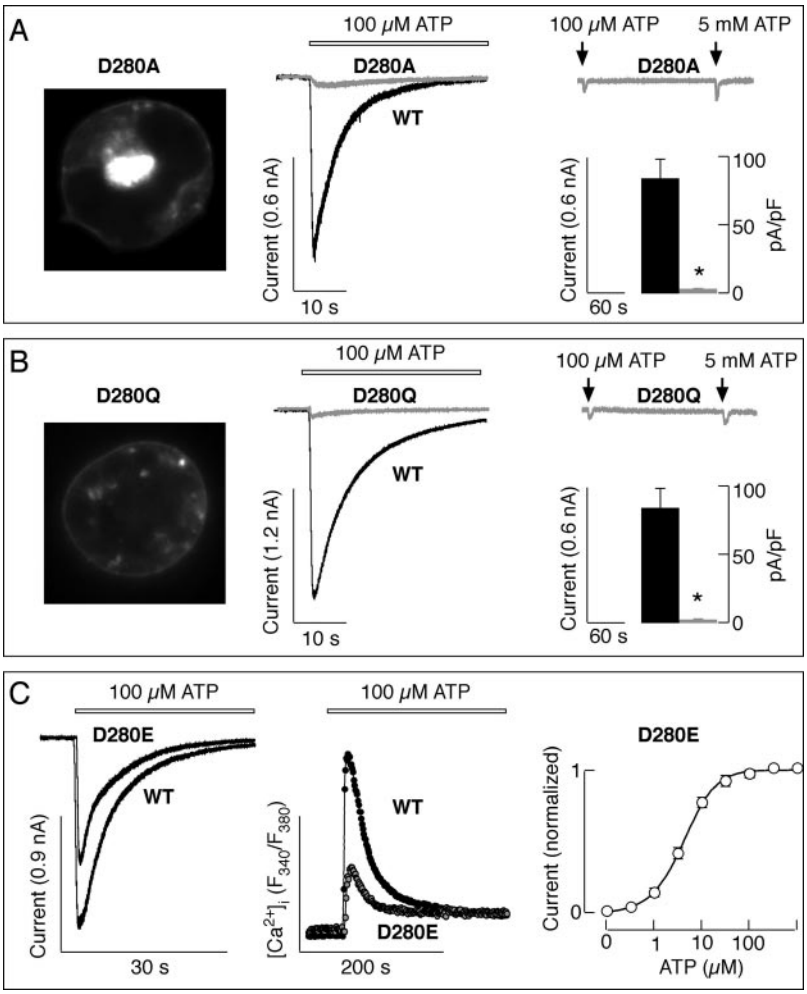

Fig. 4. Asp280 may coordinate ATP binding via the magnesium at $P2X_4R$. A and B, loss of $P2X_4R$ function by replacement of Asp280 with the noncharged alanine (A) and glutamine (B) residues. Left, expression pattern of mutant receptors. Center, currents recorded in response to 100 μM ATP stimulation in wild-type (black traces) and mutant (gray traces) receptors. Right, dose-dependent effects of ATP on peak current response and mean values for peak current responses in controls (■) and mutant receptors (▨). Traces shown are representative of at least seven experiments per channel. C, rescue of function by replacing the Asp280 residue with negatively charged glutamine. Typical patterns of current (left) and calcium (center) signals in response to 100 μM ATP of wild-type (black traces) and mutant (gray traces) receptors when expressed in HEK293 (current) and GT1–7 (calcium) cells. Right, dose-dependent effect of ATP on peak current response in cells expressing mutant receptor. In all, bars and circles are mean ± S.E.M. values; ⋆, significant difference between controls and mutants, $P < 0.01$. Vertical arrows indicate the moments of a transient (4-s) ATP application, and horizontal bars indicate the duration of sustained agonist application.

ate these bridges, because both pairs of cysteines were located close to each other. This provides another indication that the 180 to 326 fragment of $P2X_4R$ ectodomain adopts the suggested β-pleated sheet fold.

Characterization of Mutants Predicted by Three-Dimensional Model. To test the validity of the three-dimensional model predictions for the roles of Arg278 in γ-phosphate binding and His286, Lys258, and/or Asn287 residues in β-phosphate coordination, these amino acids were mutated, and mutants were characterized. Experiments with R278A and R278K mutants supported the relevance of this residue in ATP binding. As shown in Fig. 7A, the R278A mutant was expressed at the plasma membrane (left) and responded to application of 100 μM ATP (center left), 2-MeS-ATP, and BzATP (data not shown) with a small current. The rightward shift in the sensitivity of R278A receptor to ATP probably accounted for a decrease in peak current response, because there was an increase in current amplitude when cells were stimulated with 5 mM ATP (Fig. 7A, center right). The replacement of arginine with lysine gave a functional channel, responding to ATP in a micromolar concentration range (Fig. 7A, right) and with an estimated EC_{50} value shifted slightly leftward from the EC_{50} values of wild-type channels (Table 1). The peak current amplitude of mutant channel was significantly reduced (Fig. 7A, center left, and Table 1), whereas the rate of receptor desensitization was not affected (Table 1).

Mutation of Lys258 and Asn287 to alanine did not affect the function of channels, as illustrated by EC_{50} values, peak current responses, and rates of receptor desensitization (Table 1). In contrast, experiments with rat $P2X_4R$ expressed in HEK293 cells confirmed the effects of external pH on signaling. Changing the external pH from 7.35 to 6.5 reduced the peak current amplitude, whereas an increase in pH to 8 enhanced it (Fig. 7B, bottom left). The H286A-$P2X_4$ mutant was functional when expressed in HEK293 cells and exhibited sensitivity to ATP similar to wild-type channels (Fig. 7B, right) that is consistent with literature data (Xiong et al., 2004). The rate of mutant receptor desensitization was comparable with wild-type channel (Table 1) when experiments were performed in cells bathed in a medium with pH 7.35. Furthermore, there was no change in the current amplitude with changes in extracellular pH, in contrast to the wild-type channel. Figure 7B, top left, shows typical traces of current responses by mutant receptor stimulated with 3 μM ATP, and Fig. 7B, center, shows the lack of effects of acidification on peak current in H286A mutant, confirming that pH sensitivity resides in the rat $P2X_4$ channel protein.

Discussion

The extracellular loop of P2XRs contains a sequence stretch in positions 170 to 330 that exhibits similarities with the catalytic domains of class II aminoacyl-tRNA synthetases (Freist et al., 1998). From this sequence alignments and secondary structure predictions, five residues emerged as potentially relevant for ATP binding at P2XRs: Lys190, Lys197, Phe230, Asp280, and Arg318 ($P2X_4$ counting). Here, we show that mutation of three of these residues, Lys190, Phe230, and Asp280, severely affected $P2X_4R$ function, supporting this model. The behavior of two $P2X_2R$ mutants is also consistent with the model. However, of $P2X_1R$-R314, the potential residue for recognition of γ-phosphate (Ennion et al., 2000), and Phe230, the potential residue for adenosine recognition (Roberts and Evans, 2004), did not affect the efficacy of ATP for $P2X_4R$. Our experimental data also do not support a role of Lys197 in ATP action and question a role of Arg318 in ATP binding. A partial agreement of experimental data with Freist's model prompted us to build a three-dimensional model of $P2X_4R$. According to our model, the 180 to 326 fragment of rat $P2X_4$ ectodomain adopts a six-stranded antiparallel β-pleated sheet structure and contains the ATP binding site. As discussed below, our model also provided a rationale for the observed compatibility and differences be-

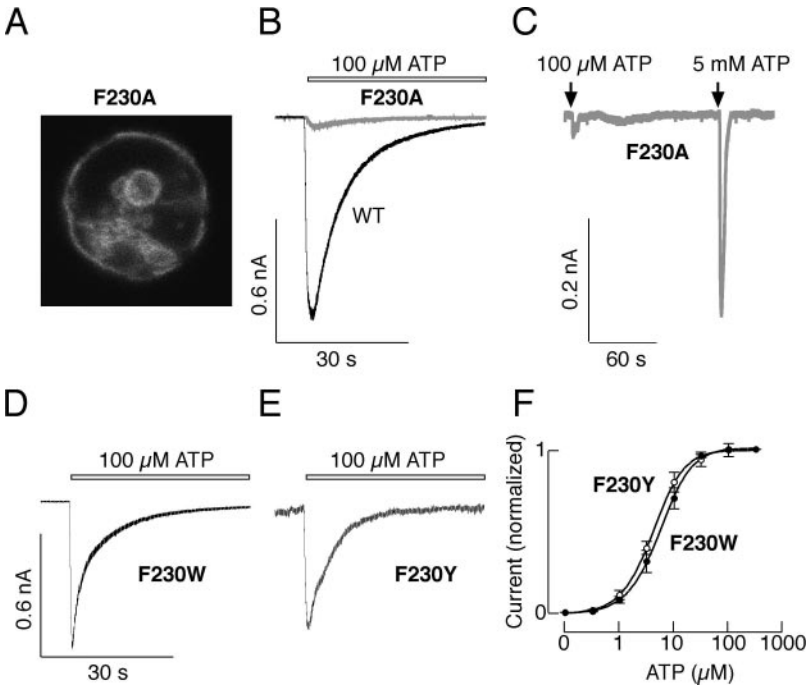

Fig. 5. Potential role of Phe230 residue of $P2X_4R$ in recognition of adenine group of ATP. A, expression pattern of the F230A mutant. B, typical patterns of current signals in wild-type (black trace) and F230A mutant receptors (gray trace). C, dose-dependent effects of ATP on peak current response by F230A mutant. D and E, typical patterns of 100 μM ATP-induced current signals by F230W and F230Y mutants. F, dose-dependent effects of ATP on peak current response by F230W and F230Y mutants. Data points are mean $\pm$ S.E.M. values, with $n = 8$ per channel. Vertical arrows indicate the moments of a transient (4-s) ATP application, and horizontal bars indicate the duration of sustained agonist application.

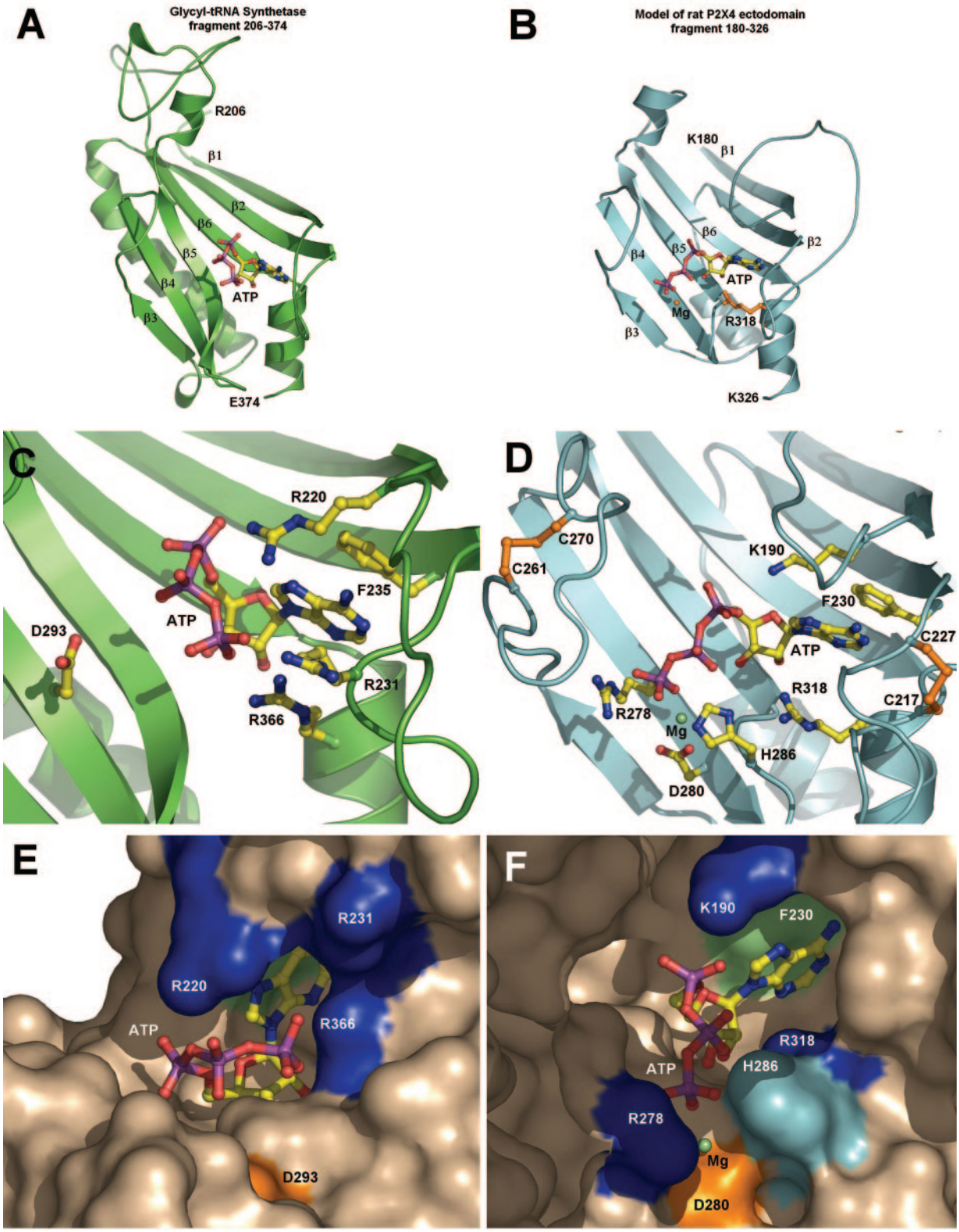

Fig. 6. Structural similarities of 185 to 323 ectodomain sequences of P2XRs with class II aminoacyl-tRNA synthetases. A, the X-ray structure of catalytic domain of glycyl-tRNA synthetase (fragment 206–374, PDB code 1B76) with bound ATP. The crystal structures of this and two other aminoacyl-tRNA synthetases were used as templates for homology modeling of the rat $P2X_4$ ectodomain. B, model of rat $P2X_4$ ectodomain (fragment 180–326). C, residues important for ATP binding by glycyl-tRNA synthetase (PDB access code 1B76). D, residues of rat $P2X_4$ predicted to be involved in ATP and magnesium ion binding. Residues Lys190, Phe230, Asp280, and Arg318 of $P2X_4$ correspond to Arg220, Phe235, Asp293, and Arg366 in the enzyme structure, respectively. Two disulfide bridges of rat $P2X_4$, Cys217–Cys227 and Cys261–Cys270, are shown in orange. E and F, surface representation of ATP binding pocket of glycyl-tRNA synthetase with bound ATP (E) and ATP binding site of modeled rat $P2X_4$ ectodomain with docked molecule of ATP (F). Labeled amino acid residues are predicted to be involved in ATP binding. Blue and gray indicate positively charged residues, whereas orange indicates negatively charged residues.

tween Freist's alignment model and the majority of experimental observations.

Many ATP-binding proteins bind ATP complexed with magnesium cations, which usually stabilizes the conformation of ATP and/or represents structural parts of the active site and participates in catalysis. Therefore, negatively charged amino acids are often found to participate in ATP binding via this cation, including II aminoacyl-tRNA synthetases (Arnez et al., 1997). In Freist's alignment model the corresponding residue for Mg^{2+} binding at $P2X_4R$ is Asp280, and in our three-dimensional model, this residue is an integral component of ATP binding pocket. The relevance of this negatively charged residue on ATP-induced currents in other P2XRs has not been studied previously. We may speculate the broader relevance of negatively charged residues among channels because five receptors have aspartic acid at the corresponding position, whereas the corresponding residue at $P2X_1R$ and $P2X_6R$ is glutamic acid. In II aminoacyl-tRNA synthetases, both the aspartic and glutamic acid residues at the corresponding position mediate the recognition of the ATP-magnesium complex. In both classes of these enzymes, the stabilizing role of magnesium is best exemplified by the two ions bridging the β- and γ-phosphates (Arnez et al., 1999). In nonphysiological concentrations (2–10 mM), Mg^{2+} exhibits additional effects on ATP-induced $P2X_4R$ current. It inhibits the ATP-gated ion channel function by decreasing the affinity of the agonist binding (Li et al., 1997), an effect probably resulting from changing the balance between positive and negative charges at the ligand binding pocket. Single-channel recording from cells expressing $P2X_4R$ also showed inhibitory effects of high $[Mg^{2+}]$ in reducing the amplitude of single-channel current, an observation consistent with a fast channel block, and reducing the mean opening time, suggesting an effect on ion gating (Negulyaev and Markwardt, 2000).

In general, positively charged ectodomain residues could interact with negative phosphate groups of ATP and coordinate the binding of the phosphate chain of this agonist. Both the alignment and three-dimensional models predict a role of Lys190 in recognition of α-phosphate. Experiments with $P2X_1R$ (Ennion et al., 2000), $P2X_2R$ (Jiang et al., 2000), and $P2X_4R$ (present study) are in general agreement with this prediction. On the other hand, there is a large loop between the β1 and β2 strands in the channel sequence in our model, whereas the class II aminoacyl-tRNA synthetases possesses just a relatively short loop between these two strands. The extension of this loop misplaces the Lys197 residue, and its function is substituted by β4-strand residue Arg278. Consistent with the model prediction, mutation of the Lys197 residue did not affect ATP potency at $P2X_4R$, whereas the R278A mutant, but not the R278K mutant, showed a dramatic decrease in the sensitivity to ATP. Furthermore, the three-dimensional model indicates a role of His286 in ATP binding, whereas Freist's model does not identify a residue for the recognition of a β-phosphate group. The His286 residue is unique for $P2X_4R$. Earlier studies have indicated that acidification causes a rightward shift in the ATP concentration-response curves for $P2X_4R$ (Wildman et al., 1999) and that mutation of the His286 residue of the human $P2X_4R$ completely abolished the pH sensitivity of this receptor at all agonist concentrations when the *Xenopus laevis* oocyte expression system was used (Clarke et al., 2000). Our results with the rat H286-$P2X_4R$ mutant are consistent with these findings.

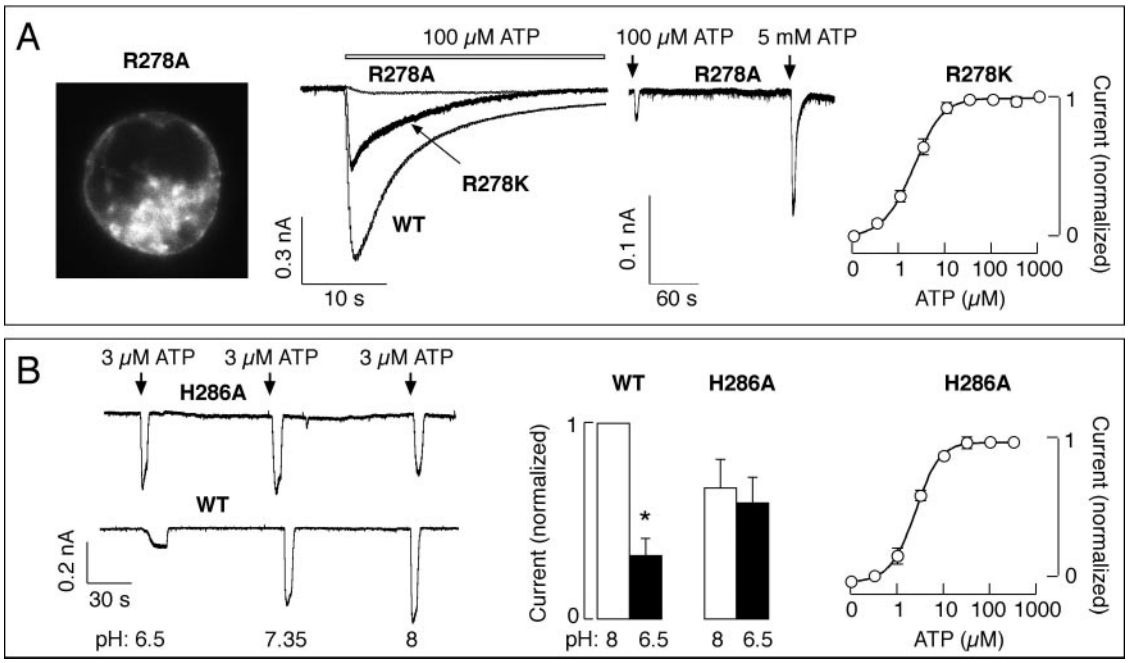

Fig. 7. Positively charged residues and detection of the phosphate chain of ATP. A, characterization of Arg278 mutant receptors. Left, the expression pattern of mutant receptors. Center left, typical patterns of current signals of wild-type and mutant receptors in response to 100 μM. Center right, current responses to two ATP concentrations. Right, dose-dependent effects of ATP on peak current response by rescue mutants. Data points are means ± S.E.M. values with $n = 7$. B, mutation of His286 removes extracellular pH sensitivity of receptor expressed in HEK293 cells. Left, typical currents of wild-type (bottom trace) and mutant (top trace) receptors in response to 3 μM ATP stimulation. Center, comparison of the peak current amplitude for wild-type and mutant receptors in response to 3 μM ATP at pH 8.0 (□) and 6.5 (■). Right, dose-dependent effects of ATP on peak current response by H286A mutant. Vertical arrows indicate the initiation of a transient (4-s) ATP application, and horizontal bars indicate the duration of sustained agonist applications.

In addition, Freist's model suggests that the Arg318 residue of $P2X_4R$ together with Lys197 residue participates in coordination of the γ-phosphate moiety of ATP. In our three-dimensional model, however, Arg318 residue is located just next to the His286 residue and could be in contact with deoxyribose ring of ATP. Moreover, Arg318 is an integral residue of the α-helix directed toward the second plasma-membrane domain (Fig. 6B) and could participate in molecular signal transduction from ATP binding pocket toward the second transmembrane domain. As revealed recently, this could be relevant for conformation changes in the pore that occur during receptor activation (Li et al., 2004). Experiments with $\alpha\beta$-MeATP, a partial agonist for $P2X_4R$, are in general agreement with the second hypothesis, but additional studies are needed to clarify this issue. Finally, of potential interest for discussion is the diversity in the structure and length of the chain between Phe276 and Tyr292 ($P2X_4$ numbering) among P2XRs. In our model, this region of $P2X_4R$ accounts for the parts of $\beta4$ and $\beta5$ strands and the interconnecting loop and contains three of five residues involved in ATP binding. We may speculate that such variability in the sequence structure reflects on agonist specificity and efficacy among receptors.

The site of detection of the adenine group gives nucleotide selectivity to the P2XRs, and in many ATP binding proteins, aromatic amino acids mediate the recognition of this group. For example, phenylalanine coordinates the recognition of adenine group of ATP by DEAD box helicases (Tanner et al., 2003). The Freist's alignment model suggested a role for Phe230 residue at $P2X_1R$ and $P2X_4R$ and the corresponding Phe227 residue at $P2X_2R$ in recognition of the adenine ring. The relevance of these two residues was tested at $P2X_1R$ and $P2X_2R$ and gave the opposite results; there was no change in ATP-induced current in F230A-$P2X_1R$ mutant compared with wild-type channels (Roberts and Evans, 2004), whereas the responsiveness to ATP was abolished in F227L-$P2X_2R$ and F207I-$P2X_2R$ mutants (Nakazawa et al., 2004). We also observed dramatic effects of Phe230 mutation at $P2X_4R$, and this residue seems to be sufficient in coordination of the binding of the adenine ring. Single aromatic residues also coordinate the binding of the adenine ring in class II aminoacyl-tRNA synthetases (Arnez et al., 1997) and P-type ATPases (Toyoshima and Mizutani, 2004). Multiple sequence alignment of P2XR channels shows that subunits other than $P2X_1$ contain a basic residue (arginine or lysine) just next to Phe230, whereas $P2X_1$ sequences have asparagine, serine, or glutamine residues at this position. This could account for differences in experiments with site-directed mutagenesis.

As discussed recently (Vial et al., 2004), mutagenesis may change the ATP potency (indicated by changes in EC_{50} values), the response amplitude, and/or the time course, but it may also result in loss of function. Changes in EC_{50} values may reflect changes in the ATP binding affinity, whereas changes in gating/channel properties of the receptors may reflect on the time course of responses (i.e., activation, deactivation, and desensitization kinetics). On the other hand, the trafficking of receptors or the proper assemble of subunits at the plasma membrane may affect the amplitude of response or underlie the loss of function. In mutation studies, the GFP-tagged $P2X_4$ and confocal microscopy were used to identify their expression pattern in HEK293 cells. We believe that GFP fluorescence at the plasma membrane and the parallelism in the behavior of GFP-tagged and nontagged receptors expressed in HEK293 and GT1–7 cells provides sufficient qualitative information about the plasma membrane expression of mutants and that a decrease in receptor function reflects the potential importance of targeted residues for ATP binding and/or gating rather than the problems in the trafficking of receptors. This conclusion was further supported by a finding published previously that a conserved motif in the cytoplasmic C termini of P2X subunits is necessary for their plasma membrane expression (Jiang et al., 2003), and by our finding that preservation of charged or aromatic residues "rescued" the channel function. To this end, all mutant receptors responded to ATP when applied in a low millimolar concentration range, indicating that mutant subunits form functional plasma membrane channels but with low sensitivity to ATP.

Acknowledgments

Confocal imaging was performed at the Microscopy and Imaging Core (National Institute of Child Health and Human Development, National Institutes of Health, Bethesda, MD) with the assistance of Dr. Vincent Schram.

References

Arnez JG, Augustine JG, Moras D, and Francklyn CS (1997) The first step of aminoacylation at the atomic level in histidyl-tRNA synthetase. *Proc Natl Acad Sci USA* **94:**7144–7149.

Arnez JG, Dock-Bregeon AC, and Moras D (1999) Glycyl-tRNA synthetase uses a negatively charged pit for specific recognition and activation of glycine. *J Mol Biol* **286:**1449–1459.

Belrhali H, Yaremchuk A, Tukalo M, Larsen K, Berthet-Colominas C, Leberman R, Beijer B, Sproat B, Als-Nielsen J, Grubel G, et al. (1994) Crystal structures at 2.5 angstrom resolution of seryl-tRNA synthetase complexed with two analogs of seryl adenylate. *Science (Wash DC)* **263:**1432–1436.

Bobanovic LK, Royle SJ, and Murrell-Lagnado (2002) P2X receptor trafficking in neurons is subunit specific. *J Neurosci* **22:**4814–4824.

Clarke CE, Benham CD, Bridges A, George AR, and Meadows HJ (2000) Mutation of histidine 286 of the human P2X4 purinoceptor removes extracellular pH sensitivity. *J Physiol (Lond)* **523 (Pt 3):**697–703.

Clyne JD, LaPointe LD, and Hume RI (2002a) The role of histidine residues in modulation of the rat $P2X_2$ purinoceptor by zinc and pH. *J Physiol (Lond)* **539:** 347–359.

Clyne JD, Wang LF, and Hume RI (2002b) Mutational analysis of the conserved cysteines of the rat P2X2 purinoceptor. *J Neurosci* **22:**3873–3880.

Coddou C, Morales B, Gonzalez J, Grauso M, Gordillo F, Bull P, Rassendren F, and Huidobro-Toro JP (2003) Histidine 140 plays a key role in the inhibitory modulation of the P2X4 nucleotide receptor by copper but not zinc. *J Biol Chem* **278:** 36777–36785.

Ennion S, Hagan S, and Evans RJ (2000) The role of positively charged amino acids in ATP recognition by human P2X1 receptors. *J Biol Chem* **275:**29361–29367.

Ennion SJ, Ritson J, and Evans RJ (2001) Conserved negatively charged residues are not required for ATP action at $P2X_1$ receptors. *Biochem Biophys Res Commun* **289:**700–704.

Eriani G, Cavarelli J, Martin F, Ador L, Rees B, Thierry JC, Gangloff J, and Moras D (1995) The class II aminoacyl-tRNA synthetases and their active site: evolutionary conservation of an ATP binding site. *J Mol Evol* **40:**499–508.

Fabbretti E, Sokolova E, Masten L, D'Arco M, Fabbro A, Nistri A, and Giniatullin R (2004) Identification of negative residues in the P2X3 ATP receptor ectodomain as structural determinants for desensitization and the Ca^{2+} sensing modulatory sites. *J Biol Chem* **279:**53109–53115.

Freist W, Verhey JF, Stuhmer W, and Gauss DH (1998) ATP binding site of P2X channel proteins: structural similarities with class II aminoacyl-tRNA synthetases. *FEBS Lett* **434:**61–65.

Guex N and Peitsch MC (1997) SWISS-MODEL and the Swiss-PdbViewer: an environment for comparative protein modeling. *Electrophoresis* **18:**2714–2723.

Hassinen T and Perakyla M (2001) New energy terms for reduced protein models implemented in an off-lattice force field. *J Comput Chem* **22:**1229–1242.

He ML, Zemkova H, Koshimizu TA, Tomic M, and Stojilkovic SS (2003a) Intracellular calcium measurements as a method in studies on activity of purinergic P2X receptor channels. *Am J Physiol* **285:**C467–C479.

He ML, Zemkova H, and Stojilkovic SS (2003b) Dependence of purinergic P2X receptor activity on ectodomain structure. *J Biol Chem* **278:**10182–10188.

Hu B, Senkler C, Yang A, Soto F, and Liang BT (2002) P2X4 receptor is a glycosylated cardiac receptor mediating a positive inotropic response to ATP. *J Biol Chem* **277:**15752–15757.

Jiang LH, Kim M, Spelta V, Bo X, Surprenant A, and North RA (2003) Subunit arrangement in P2X receptors. *J Neurosci* **23:**8903–8910.

Jiang LH, Rassendren F, Surprenant A, and North RA (2000) Identification of amino acid residues contributing to the ATP-binding site of a purinergic P2X receptor. *J Biol Chem* **275:**34190–34196.

Jones DT (1999) Protein secondary structure prediction based on position-specific scoring matrices. *J Mol Biol* **292:**195–202.
Jones TA, Zou JY, Cowan SW, and Kjeldgaard (1991) Improved methods for building protein models in electron density maps and the location of errors in these models. *Acta Crystallogr A* **47:**110–119.
Katchalski-Katzir E, Shariv I, Eisenstein M, Friesem AA, Aflalo C, and Vakser IA (1992) Molecular surface recognition: determination of geometric fit between proteins and their ligands by correlation techniques. *Proc Natl Acad Sci USA* **89:** 2195–2199.
Khakh BS, Proctor WR, Dunwiddie TV, Labarca C, and Lester HA (1999) Allosteric control of gating and kinetics at $P2X_4$ receptor channels. *J Neurosci* **19:**7289–7299.
Knofel T and Strater N (2001) Mechanism of hydrolysis of phosphate esters by the dimetal center of 5′-nucleotidase based on crystal structures. *J Mol Biol* **309:**239–254.
Koshimizu T, Koshimizu M, and Stojilkovic SS (1999) Contributions of the C-terminal domain to the control of P2X receptor desensitization. *J Biol Chem* **274:**37651–37657.
Koshimizu T, Tomic M, Koshimizu M, and Stojilkovic SS (1998) Identification of amino acid residues contributing to desensitization of the P2X2 receptor channel. *J Biol Chem* **273:**12853–12857.
Li C, Peoples RW, and Weight FF (1997) Mg^{2+} inhibition of ATP-activated current in rat nodose ganglion neurons: evidence that Mg^{2+} decreases the agonist affinity of the receptor. *J Neurophysiol* **77:**3391–3395.
Li Z, Migita K, Samways DS, Voigt MM, and Egan TM (2004) Gain and loss of channel function by alanine substitutions in the transmembrane segments of the rat ATP-gated P2X2 receptor. *J Neurosci* **24:**7378–7386.
Mager PP, Weber A, and Illes P (2004) Bridging the gap between structural bioinformatics and receptor research: the membrane-embedded, ligand-gated, P2X glycoprotein receptor. *Cur Top Med Chem* **4:**1657–1705.
Nakazawa K, Ojima H, Ishii-Nozawa R, Takeuchi K, and Ohno Y (2004) Amino acid substitutions from an indispensable disulfide bond affect P2X2 receptor activation. *Eur J Pharmacol* **483:**29–35.
Negulyaev YA and Markwardt F (2000) Block by extracellular Mg^{2+} of single human purinergic P2X4 receptor channels expressed in human embryonic kidney cells. *Neurosci Lett* **279:**165–168.
Newbolt A, Stoop R, Virginio C, Surprenant A, North RA, Buell G, and Rassendren F (1998) Membrane topology of an ATP-gated ion channel (P2X receptor). *J Biol Chem* **273:**15177–15182.
Nicke A, Baumert HG, Rettinger J, Eichele A, Lambrecht G, Mutschler E, and Schmalzing G (1998) P2X1 and P2X3 receptors form stable trimers: a novel structural motif of ligand-gated ion channels. *EMBO (Eur Mol Biol Organ) J* **17:**3016–3028.
North RA (2002) Molecular physiology of P2X receptors. *Physiol Rev* **82:**1013–1067.
Ralevic V and Burnstock G (1998) Receptors for purines and pyrimidines. *Pharmacol Rev* **50:**413–492.
Rettinger J, Aschrafi A, and Schmalzing G (2000) Roles of individual N-glycans for ATP potency and expression of the rat P2X1 receptor. *J Biol Chem* **275:**33542–33547.
Roberts JA and Evans RJ (2004) ATP binding at human P2X1 receptors. Contribution of aromatic and basic amino acids revealed using mutagenesis and partial agonists. *J Biol Chem* **279:**9043–9055.
Schwede T, Kopp J, Guex N, and Peitsch MC (2003) SWISS-MODEL: an automated protein homology-modeling server. *Nucleic Acids Res* **31:**3381–3385.
Sokolova E, Skorinkin A, Fabbretti E, Masten L, Nistri A, and Giniatullin R (2004) Agonist-dependence of recovery from desensitization of $P2X_3$ receptors provides a novel and sensitive approach for their rapid up or downregulation. *Br J Pharmacol* **141:**1048–1058.
Tanner NK, Cordin O, Banroques J, Doere M, and Linder P (2003) The Q motif: a newly identified motif in DEAD box helicases may regulate ATP binding and hydrolysis. *Mol Cell* **11:**127–138.
Toyoshima C and Mizutani T (2004) Crystal structure of the calcium pump with a bound ATP analogue. *Nature (Lond)* **430:**529–535.
Vial C, Roberts JA, and Evans RJ (2004) Molecular properties of ATP-gated P2X receptor ion channels. *Trends Pharmacol Sci* **9:**487–493.
Wildman SS, King BF, and Burnstock G (1999) Modulation of ATP-responses at recombinant rP2X4 receptors by extracellular pH and zinc. *Br J Pharmacol* **126:** 762–768.
Xiong K, Stewart RR, Weight FF, and Li C (2004) Role of extracellular histidines in antagonist sensitivity of the rat P2X4 receptor. *Neurosci Lett* **367:**197–200.
Zemkova H, He ML, Koshimizu TA, and Stojilkovic SS (2004) Identification of ectodomain regions contributing to gating, deactivation and resensitization of purinergic P2X receptors. *J Neurosci* **24:**6968–6978.

Address correspondence to: Dr. Stanko S. Stojilkovic, ERRB/NICHD, Building 49, Room 6A-36, 49 Convent Drive, Bethesda, MD 20892-4510. E-mail: stankos@helix.nih.gov